Biochimica et Biophysica Acta 1837 (2014) 264–269

Contents lists available at ScienceDirect

Biochimica et Biophysica Acta

journal homepage: www.elsevier.com/locate/bbabio

Fluorescence kinetics of PSII crystals containing Ca^{2+} or Sr^{2+} in the oxygen evolving complex☆

Bart van Oort [a,*], Joanna Kargul [b], James Barber [c], Herbert van Amerongen [d]

[a] Department of Physics and Astronomy, Faculty of Sciences, VU University Amsterdam, De Boelelaan 1081, 1081 HV Amsterdam, The Netherlands
[b] Department of Plant Molecular Physiology, Faculty of Biology, University of Warsaw, Miecznikowa 1, 02-096 Warsaw, Poland
[c] Division of Molecular Biosciences, Faculty of Natural Sciences, Imperial College London, London SW7 2AZ, UK
[d] Laboratory of Biophysics, Wageningen University, P. O. Box 8128, 6700 ET Wageningen, The Netherlands

ARTICLE INFO

Article history:
Received 6 October 2013
Received in revised form 6 November 2013
Accepted 12 November 2013
Available online 20 November 2013

Keywords:
Photosystem II
Fluorescence lifetime imaging
FLIM
Picosecond fluorescence
Crystallography
Ca^{2+}/Sr^{2+} exchange

ABSTRACT

Photosystem II (PSII) is the pigment–protein complex which converts sunlight energy into chemical energy by catalysing the process of light-driven oxidation of water into reducing equivalents in the form of protons and electrons. Three-dimensional structures from x-ray crystallography have been used extensively to model these processes. However, the crystal structures are not necessarily identical to those of the solubilised complexes. Here we compared picosecond fluorescence of solubilised and crystallised PSII core particles isolated from the thermophilic cyanobacterium *Thermosynechococcus elongatus*. The fluorescence of the crystals is sensitive to the presence of artificial electron acceptors ($K_3Fe(CN)_3$) and electron transport inhibitors (DCMU). In PSII with reaction centres in the open state, the picosecond fluorescence of PSII crystals and solubilised PSII is indistinguishable. Additionally we compared picosecond fluorescence of native PSII with PSII in which Ca^2 in the oxygen evolving complex (OEC) is biosynthetically replaced by Sr^{2+}. With the Sr^{2+} replaced OEC the average fluorescence decay slows down slightly (81 ps to 85 ps), and reaction centres are less readily closed, indicating that both energy transfer/trapping and electron transfer are affected by the replacement.

1. Introduction

Primary steps of the photosynthetic conversion of solar energy into chemical energy occur in the membrane-bound photosystems, photosystem I (PSI) and photosystem II (PSII[1]). These photosystems are highly organised pigment–protein complexes embedded within photosynthetic membranes. In oxygenic photosynthesis, two photosystems work in series to extract electrons from the substrate water molecules and transfer them to the final acceptor, $NADP^+$ via a series of redox-active cofactors.

PSII catalyses the thermodynamically challenging process of light-driven oxidation of water into reducing equivalents in the form of protons and electrons. As a by-product of this reaction, molecular oxygen is released that sustains all forms of aerobic life on Earth. The primary ultrafast photochemical reactions in PSII occur within its reaction centre (RC) composed of the D1 and D2 subunits which bind most of the redox-active electron transport cofactors. The PSII inner antenna subunits CP43 and CP47 together bind 29 chlorophyll (Chl) *a* molecules, which, after light absorption, transfer excitons to the primary electron donor in the RC, followed by charge separation on a picosecond timescale [1–8]. Subsequent oxidation of the so-called P680 to a highly oxidising cationic radical $P680^{\bullet+}$ drives a concomitant water splitting reaction at the oxygen evolving complex (OEC). The reduction of oxidised $P680^{\bullet+}$ using water-derived electrons is aided by the redox-active tyrosine Y_z of the D1 subunit. The catalytic site for water oxidation is composed of a Mn_4Ca-cluster surrounded by a number of highly conserved amino acids, mainly located in the D1 RC subunit and one from the CP43 inner antenna subunit [9–14].

Over the last decade, significant progress has been made in elucidating the PSII structure using X-ray crystallography [9–17] and a number of complementary approaches including XAS (e.g. [18–20]), EXAFS (e.g. [21–23]), EPR (e.g. [24,25]) and FTIR (e.g. [26–28]). The crystallographic analyses of the dimeric and monomeric PSII structures from the thermophilic cyanobacteria *Thermosynechococcus elongatus* and *Thermosynechococcus vulcanus* allowed for the assignment of all the 19–20 protein subunits per monomer. The latest near-atomic structure of dimeric PSII at 1.9 Å revealed that bound within the protein subunits are over 1300 water molecules and 85 cofactors including 35 Chl *a* molecules, 2 pheophytins, 11 β-carotenes, over 20 lipids, 2 plastoquinones, 2 haem irons, 1 non-haem iron, 4 Mn atoms, 3–4 Ca atoms, 3 Cl^- ions, and 1 bicarbonate [9]. The geometry of the catalytic site

* Corresponding author. Tel.: +31 20 598 6383; fax: +31 20 598 7999.
E-mail address: b.f.van.oort@vu.nl (B. van Oort).

[1] Abbreviations: CaPSII, native photosystem II; Chl, chlorophyll; FLIM, fluorescence lifetime imaging microscopy; HL, highest excitation intensity; LHCII, light harvesting complex II; LL, lowest excitation intensity; OEC, oxygen evolving complex; PSI, photosystem I; PSII, photosystem II; RC, reaction centre; SrPSII, photosystem II with Ca^{2+} in the OEC biosynthetically replaced by Sr^{2+}; TCSPC, time correlated single photon counting

0005-2728/$ – see front matter © 2013 The Authors. Published by Elsevier B.V. All rights reserved.
http://dx.doi.org/10.1016/j.bbabio.2013.11.008

resembles a distorted cubane-like structure in which three Mn ions and a Ca ion that are present at the corners of a cubane are linked with oxo-bridges, and the fourth 'dangler' Mn is connected to the cubane via bridging oxygens.

Time-resolved fluorescence is a powerful tool to obtain information on the kinetics of energy and electron transfer processes, thus providing information on the excited-state dynamics of the redox-active proteins, such as pigment-containing protein complexes [29]. The excited-state dynamics depends largely on the structure and organisation of the pigment molecules and protein subunits within these complexes. In general, multi-exponential decays have been observed in cyanobacterial PSII (e.g. [5,7]). These decays are typically described either phenomenologically, using compartmental models, or using the near atomic structure as starting point for modelling using approaches such as modified Redfield theory (e.g. [30–36]). However, it is not a priori known whether the molecular structure of solubilised PSII particles (used for optical spectroscopy) is the same as that of PSII crystals. Structure and dynamics of pigment–protein complexes may differ when compared for the solubilised and crystallised forms of such complexes. For example, the isolated light-harvesting complex II (LHCII), which functions as the outer light harvesting antenna of the higher plant PSII, shows clear differences in Raman [37] and fluorescence [37–39] parameters when solubilised particles and crystals of this protein complex are compared. Similarly, the PSII core complexes from cyanobacteria exhibit different electron transfer rates in solubilised and crystallised forms [40], and may bind different numbers of quinones per RC [41]. In addition, the fluorescence lifetimes of ethidium bromide bound to DNA and several fluorescent proteins of the GFP family are shorter when measured in crystals as compared to solubilised samples [42]. In contrast, higher plant PSI shows identical picosecond fluorescence kinetics for solubilised particles and crystals [43].

As the excited-state properties of PSII obtained from theoretical studies based on the crystal structures may differ from those in solution, we set out to compare the excited-state dynamics properties of the *T. elongatus* PSII both in the crystallised and solubilised forms of this complex. To this end, we measured picosecond fluorescence of the PSII crystals by time-domain fluorescence lifetime imaging microscopy (FLIM), and of the solubilised PSII core particles by time-correlated single photon counting (TCSPC). We demonstrate that the parameters of the excited-state dynamics are almost indistinguishable for the crystallised and solubilised forms of cyanobacterial PSII. In addition, we examined the excited-state dynamics of the native PSII (CaPSII) and its modified counterpart in which the Ca^{2+} cation in the OEC was biosynthetically replaced by Sr^{2+} (SrPSII). We show that in the open state (F_0) RCs, the fluorescence kinetics parameters are very similar for the native and modified PSII, both in the solubilised and crystallised forms. Importantly, we also demonstrate that the RCs of CaPSII are more readily closed compared to SrPSII RCs. We discuss the functional implications of the latter.

2. Materials and methods

2.1. Sample preparation

Thermosynechococcus elongatus CaPSII and SrPSII core particles and 3D crystals were prepared as described in Kargul et al. [40]. Both SrPSII and CaPSII crystals were grown at 17 °C using the hanging drop vapour diffusion method in the presence of 5–8% PEG-4000 (Fluka), 0.5 mM of methyl mercurial chloride (Hampton Research) and 0.055 mM polyoxyethylene lauryl ether ($C_{12}E_8$) (Hampton Research). For all the FLIM and TCSPC measurements, both types of crystals were harvested after 48 h of incubation at 17 °C in the dark. During harvesting crystals were cryoprotected in 25% glycerol added stepwise, as described in Kargul et al. [40]. A drop of buffer containing crystals was cast on a glass cover slide and left to sediment for several minutes before the first fluorescence lifetime imaging.

2.2. Time-correlated single photon counting (TCSPC)

Time-resolved fluorescence of PSII core particles was measured by TCSPC using a home-built setup [44]. Samples were excited by a 1-mm in diameter vertically polarised laser beam of 412 nm, 200 fs duration and 3.8 MHz repetition rate. Fluorescence was collected at a right angle to the excitation beam, and care was taken to minimise data distortion [45]. The fluorescence light was detected at magic angle polarisation through a 645 nm long pass filter (Schott RG 645) tilted by 5° to prevent reflections. Detection times were stored in a multichannel analyser (4096 channels of 2.0 ps). All measurements were performed at 287 K, and the number of counts in the peak channel was approximately 30,000. Curves were fitted to a sum of n exponential decays ($F(t) = \sum_n a_n e^{-t/\tau_n}$, with fluorescence lifetimes τ_n and relative amplitudes $p_n = a_n / \sum_n a_n$) that was convoluted with the instrument response function (IRF, ~60 ps), using home-built software [46]. The IRF was determined from the fast decay of pinacyanol chloride in methanol (6 ps) [43]. The fit quality was evaluated from the reduced χ^2, and from plots of the weighted residuals and the autocorrelation thereof.

PSII particles were suspended in a 1 × 1 cm quartz cuvette in a buffer of 20 mM MES, 10 mM $MgCl_2$, 10 mM $CaCl_2$ at pH 6.5, at an optical density of 0.1/cm at the Q_y maximum. To measure excited state dynamics of the open RCs, 200 μM $K_3Fe(CN)_6$ was added, and the samples were incubated in the dark at least half an hour before the measurement. Furthermore, the excitation intensity was reduced to 1.3 μW, with neutral density filters. At this intensity (and repetition rate and spot size, see above) each pulse excites 1 out of ~$1.3 * 10^6$ reaction centres. This means that each reaction centre absorbs fewer than 3 photons per second. This number was further reduced by continuous sample mixing with a magnetic stirrer. RCs were gradually closed by increasing the excitation intensity up to 75 μW and by omitting $K_3Fe(CN)_6$ and adding 10 μM DCMU (3-(3,4-dichlorophenyl)-1,1-dimethylurea, which inhibits electron transfer from Q_A to Q_B). As expected, no singlet–singlet and singlet–triplet annihilation were detected under these conditions.

Fluorescence kinetics of the PSII crystals were compared with those of solubilised PSII particles by construction of theoretical decay curves from the fit results of the solubilised particles and subsequent convolution with the IRF of the FLIM, using a reference convolution routine [47]. The resulting curves are compared with the FLIM data. This approach was previously successfully used for PSI [43].

2.3. Fluorescence lifetime imaging microscopy (FLIM)

Time-resolved fluorescence of PSII crystals was measured by FLIM, with the setup as previously described [48]. In short, two-photon excitation pulses (860 nm, 150 fs pulse duration, 76 MHz repetition rate) were focused onto the sample with a 60× water immersion objective lens (Nikon CFI Plan Apochromat, numerical aperture: 1.2). Fluorescence was detected via non-descanned single photon counting detection, through a band-pass filter centred at 700 nm (75 nm width) (HQ700/75 Chroma, Vermont, USA). Images of 32 × 32 pixels were obtained, with 4096 time channels of 3.1 ps. Line scan rates were 250 or 500 Hz and images were averaged for 100–300 s. Typically one crystal occupied 100 to 500 pixels of the total image. 20 CaPSII and 20 SrPSII crystals were studied, each at various excitation intensities, with and without 10 μM DCMU or 4 mM $K_3Fe(CN)_3$. Excitation intensities were typically 0.4, 0.8, 2 and 4 μW; lower intensity yielded too weak signals, and higher intensities induced sample degradation.

Fitting of the fluorescence kinetics per pixel showed little variation within individual crystals. Only under high excitation intensity with

$K_3Fe(CN)_6$ the lifetimes are slightly higher in the centre than at the edge of a crystal, which is likely due to slow diffusion of $K_3Fe(CN)_3$ into the crystal (see Section 3). Therefore, the fluorescence decay curves of all pixels within a single crystal were summed to obtain higher signal-to-noise levels. The resulting curves were fitted as described for the TCSPC curves. The instrument response function (IRF) (25 ps) was determined from the fluorescence decay of pinacyanol chloride in methanol (6 ps lifetime, [43]) measured in the same sample holder as used for the PSII crystals.

3. Results and discussion

3.1. Excitation dynamics of solubilised PSII core particles

Under conditions where all RCs are open (low excitation light intensity in the presence of $K_3Fe(CN)_3$), the fluorescence kinetics of CaPSII and SrPSII core particles were similar, as shown by the fluorescence decay traces (Fig. 1), and their fit results (Table 1). The decays of CaPSII and SrPSII were fitted independently, or globally, in which case the lifetimes were constrained to be equal in both samples but the amplitudes were allowed to vary. Both fit methods yielded very similar fit parameters and fit quality. The main decay occurs with a time constant of 46 ps, followed by slower decay processes of 0.16 ns and 0.4 ns. The additional >0.8 ns-components probably originate from a very small fraction (<0.5%) of closed RCs or from uncoupled pigments. The kinetics parameters were similar to those recently published by Miloslavina et al. [5] and van der Weij-de Wit et al. [7] (Table 1), except for the fastest components which were below the time resolution of the current setup. In SrPSII the amplitude of the fastest component is slightly lower, and the amplitude of the next two components slightly higher, resulting in an average lifetime that is 4 ps slower than that recorded for the CaPSII. It is not obvious how the Ca^{2+} to Sr^{2+} exchange can affect the trapping rate. It might be due to the structural changes of the water and hydrogen bond network around Y_D upon exchange [15]. These changes could affect the free energy generated by the initial charge separated states, leading to slower charge recombination.

Fluorescence decay traces were acquired with RCs that were gradually closed by using increasingly higher excitation light intensities in the presence of an artificial electron acceptor for Q_B^- ($K_3Fe(CN)_6$) or an inhibitor of electron transfer from Q_A to Q_B (DCMU). These traces were fitted globally, with the constraint that the fluorescence lifetimes are identical for all traces. The resulting lifetimes were 46 ps, 157 ps, 406 ps, 950 ps and 2.7 ns, values that are almost identical to those for open RCs. The relative amplitude of the fastest decay component, which is strictly associated with open RCs, was plotted for different excitation intensities and is presented in Fig. 2. As expected, both types of PSII RCs are closed more easily in the presence of DCMU as compared to $K_3Fe(CN)_3$. In both cases CaPSII RCs are closed more readily than SrPSII. This may be related to differences in electron transfer rates between CaPSII and SrPSII observed for both soluble and crystallised dimeric core complexes [40,49] (see below). Substitution of Ca^{2+} by Sr^{2+} in the OEC slows down S-state kinetics beyond S_2 and S_3 states during photosynthetic water oxidation cycle [22,49–53] but the structural basis for this phenomenon was missing until recently. The latest SrPSII crystal structure resolved at 2.1 Å showed that not only the position of Sr^{2+} was shifted by 0.1–0.2 Å towards the outside of the Mn-cluster cubane, but also that one of the putative water substrate molecules (W_3) coordinated by Ca^{2+} in the native cluster was located at a slightly larger distance from the cubane, resulting in weaker binding of W_3 by Sr^{2+} [15]. In addition, by using FTIR spectroscopy, Barry and colleagues revealed a considerable structural change around the Mn cluster during S_2-to-S_3 transition upon Sr^{2+} substitution in the PSII catalytic centre, possibly due to the shift of carboxylate ligands positioning around the Mn-cluster in Sr S_3

Table 1
Fit results of fluorescence decay curves of solubilised CaPSII and SrPSII particles. Decay curves were fitted separately, and globally with equality constraints for the fluorescence lifetimes (τ) in both curves. For comparison, two recent results [5,7] of CaPSII particles from the same organism are shown, averaged over the current detection range.

Global fit			Separate fits				CaPSII literature			
	CaPSII	SrPSII	CaPSII		SrPSII		ref. [5] [c]		ref. [7] [c]	
τ [ns][a]	p[a,b]	p	τ [ns]	p	τ [ns]	p	τ [ns]	p	τ [ns]	p
0.046	0.77	0.75	0.046	0.78	0.046	0.75	0.041	0.77	0.049	0.80
0.156	0.18	0.19	0.165	0.18	0.156	0.19	0.105	0.15	0.223	0.17
0.40	0.04	0.05	0.43	0.04	0.40	0.05	0.332	0.07		
1.1	0.004	0.005	0.90	0.004	1.1	0.005				
2.9	0.0004	0.001	2.1	0.001	2.9	0.001	2.0	0.01	1.4	0.03
τ_{avg} [ns][d]	0.081	0.085	0.081		0.084		0.072		0.079	

[a] 67% confidence intervals, calculated by the exhaustive search method [55], are ≤3% for all τ and p.
[b] Relative amplitude ($p_n = a_n/\Sigma_n a_n$, with a_n the fitted amplitudes).
[c] Faster components (2 and 9 ps in [5] and 0.7 and 12 ps in [7]) are not resolved here.
[d] Average fluorescence lifetime ($\tau_{avg} = \Sigma_n p_n\tau_n/\Sigma_n p_n$) calculated without the ≥0.9 ns components.

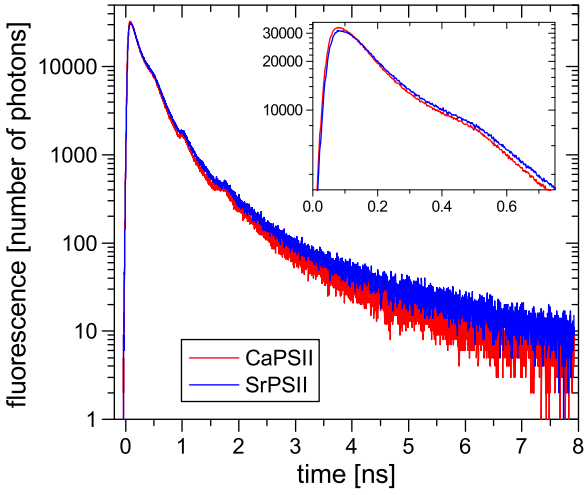

Fig. 1. Fluorescence decay kinetics of solubilised CaPSII and SrPSII particles. Fluorescence was measured with TCSPC at 287 K under conditions in which >99% of RCs are in an open state (see Materials and Methods section). The inset shows a close-up near time = 0. The curves were measured until an equal total number of detected photons was obtained. Excitation was at 412 nm and detection above 645 nm.

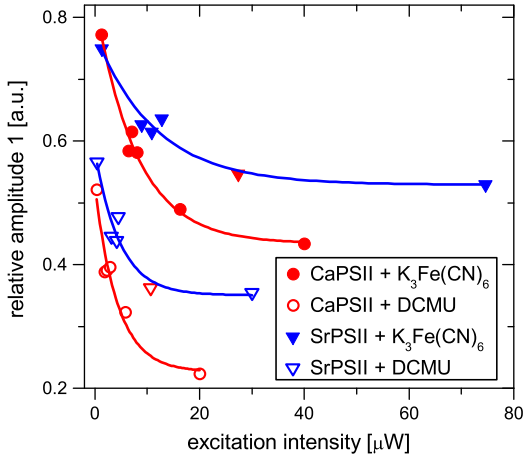

Fig. 2. Relative amplitude of the fastest fluorescence decay component (46 ps) of solubilised CaPSII and SrPSII particles as a function of light intensity (symbols), and exponential fits thereof (curves). Datasets were analysed globally, constraining lifetimes to equality for all data sets. Measurements were performed in the presence of 200 μM $K_3Fe(CN)_6$ or 10 μM DCMU, as indicated in the legend.

state [27,28,54]. All these structural changes result in overall slower S-state kinetics and a decreased oxygen evolution rate of the Sr^{2+}-substituted PSII observed in previous studies [40,49–53]. Some of us have previously shown that in Sr^{2+}-substituted PSII, forward electron transfer from the Mn_4Sr-cluster to Q_A and from Q_A^- to Q_B on the acceptor side of the complex is also slowed down, concomitant with stabilisation of the $S_2Q_A^-$ charge recombination state (backward electron transfer) [40]. It is therefore feasible that the stabilisation of the $S_2Q_A^-$ charge-separated state observed for SrPSII [40] may lead to an improved recovery of the SrPSII RC to the open state, and therefore less efficient closure of the SrPSII RC compared to the native counterpart. Quantification of the recovery rate of RCs to the open state will require detailed molecular modelling (e.g. QM/MM or DFT).

3.2. Excitation dynamics of PSII crystals

We compared excitation dynamics of Sr- and CaPSII complexes with open and partially closed RCs using time-resolved fluorescence lifetime imaging microscopy (FLIM) of both types of PSII crystals. FLIM images of the CaPSII and SrPSII crystals with open RCs were analysed by fitting of the fluorescence decay curves in each pixel to single-exponential decay functions. Typical results of single CaPSII and SrPSII crystals are presented in Fig. 3, where the colour codes for the fluorescence lifetime and the frequency histogram shows the distribution of lifetimes. Both types of PSII crystals showed similar fluorescence decay kinetics for open RC states. As for each examined Ca/SrPSII crystal, the fluorescence lifetime kinetics were homogeneous, we summed the signal over all pixels within a single crystal to increase the signal-to-noise ratio.

As shown in Fig. 4, the summed traces of fluorescence decay were similar for CaPSII and SrPSII crystals, as well as the solubilised PSII core complexes. The lower signal-to-noise ratio of the FLIM data precluded the direct determination of the five fluorescence lifetimes observed for solubilised particles. Instead, three lifetimes were resolved in two global fits (CaPSII and SrPSII) of all decay curves measured under the highest and lowest light intensity in presence or absence of $K_3Fe(CN)_3$ and DCMU (Table 2 and Supplementary Table S1). The lifetimes of Sr/CaPSII crystals were very similar, and appeared as intermediates of the five lifetimes determined for the solubilised particles: ~0.1 ns (between 0.046 and 0.156 ns), ~0.5 ns (0.4 and 1 ns) and ~2 ns. The fastest component contributes most to the decay, in qualitative agreement with the solubilised particles. This was quantitatively analysed by fitting the decay curves of the crystals while keeping the lifetimes fixed to the values obtained for the solubilised particles. The resulting relative

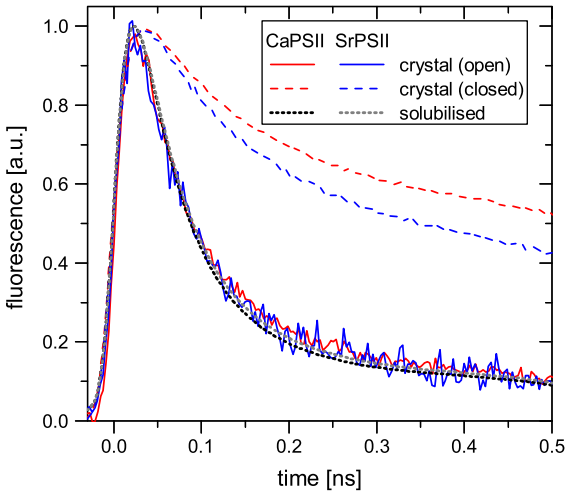

Fig. 4. Fluorescence decay kinetics of CaPSII (red) and SrPSII (blue) crystals, as measured by FLIM. Decay curves of PSII crystals with the open-state (solid lines; lowest excitation intensity + 4 mM $K_3Fe(CN)_3$) or closed-state (dashed lines; highest excitation intensity + 10 μM DCMU) RCs were obtained at room temperature using FLIM. Excitation was at 860 nm, and detection at 670–730 nm. Decay curves of open solubilised PSII (dotted lines; black CaPSII, grey SrPSII) were reconstructed from the fluorescence kinetics from TCSPC (Table 1), by convolution of the multi-exponential decay with the FLIM IRF. All curves are normalised at the peak intensity.

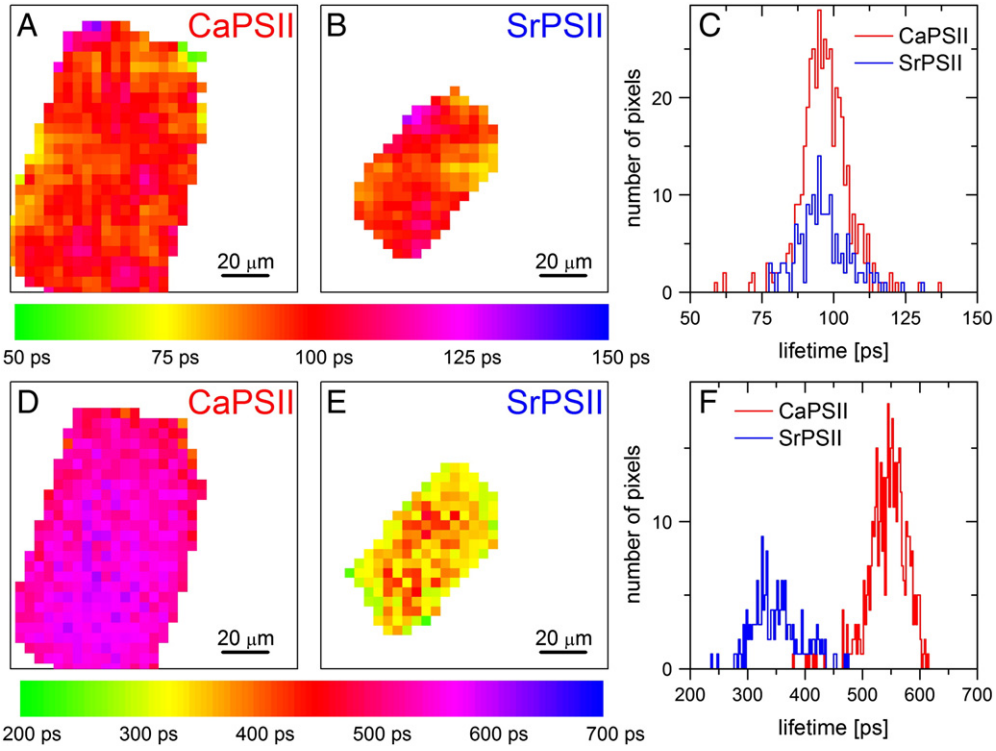

Fig. 3. Fluorescence lifetime imaging of CaPSII (A,D) and SrPSII (B,E) crystals, with false colour coding of the lifetimes from a mono-exponential fit (A,B) or average fluorescence lifetimes from a bi-exponential fit (D,E), and frequency histograms of the (average) fluorescence lifetimes (C,F). Measurements were taken at room temperature in the presence of 4 mM $K_3Fe(CN)_6$, with detection at 670–730 nm and two-photon excitation at 860 nm at the lowest (A–C) and highest (D–F) excitation intensities.

Table 2
Fit results of fluorescence decay curves of CaPSII and SrPSII crystals. Decay curves were fitted by global analysis with equality constraints on the fluorescence lifetimes (τ) of all CaPSII and all SrPSII decay curves measured at highest (HL) and lowest (LL) excitation intensity, with and without additives (4 mM $K_3Fe(CN)_3$ or 10 μM DCMU). Here we show a subset of the fit results, with mainly open (LL + $K_3Fe(CN)_3$) and closed (HL + DCMU) RCs. The complete fit results are provided as Supplementary Table S1. Fit results with lifetimes fixed to those of solubilised PSII particles (see Table 1) are also shown.

	Global fit					Lifetimes from solubilised PSII particles				
	Open			Closed		Open			Closed	
	τ [ns]	$p^{a,b}$	σ^c	$p^{a,b}$	σ	τ [ns][d]	$p^{a,e}$	σ	$p^{a,e}$	σ
CaPSII	0.13	0.93	0.02	0.34	0.06	0.046	0.67	0.03	0.02	0.04
	0.76	0.07	0.02	0.41	0.02	0.156	0.21	0.02	0.34	0.03
	2.1	0.00	0.00	0.25	0.06	0.40	0.11	0.02	0.06	0.07
						1.1 [f]	0.016	0.012	0.45	0.06
						2.9 [f]	0.0002	0.0002	0.13	0.03
SrPSII	0.11	0.91	0.03	0.37	0.08	0.046	0.63	0.03	0.10	0.08
	0.51	0.07	0.04	0.42	0.03	0.156	0.22	0.02	0.36	0.04
	1.5	0.01	0.01	0.22	0.06	0.40	0.11	0.02	0.17	0.04
						1.1 [f]	0.021	0.007	0.33	0.08
						2.9 [f]	0.0001	0.0001	0.04	0.01

[a] Relative amplitude ($p_n = a_n/\Sigma_n a_n$, with a_n the fitted amplitudes).
[b] 67% confidence intervals, calculated by the exhaustive search method [55], are smaller than σ.
[c] Standard deviation of p from 3 to 8 different crystals.
[d] Fixed.
[e] 67% confidence intervals calculated by the exhaustive search method are <20%.
[f] Amplitudes of these components are hard to estimate due to background noise.

amplitudes are very similar to those of the solubilised particles (compare Table 1 with Table 2, right). For a more direct comparison of the kinetics in PSII crystals and solubilised core particles, fluorescence decay curves were reconstructed from the fluorescence decay kinetics of open RCs in the solubilised PSII particles (Table 1), and convoluted with the instrument response function (IRF) of the FLIM setup. These reconstructed curves (Fig. 4, black and grey) are nearly indistinguishable from the experimental curves obtained for the crystals. Together, these results indicate that (within the time resolution obtained) the excited state kinetics of PSII with open RCs is identical for crystals and solubilised particles of Sr/CaPSII.

Upon illumination with higher light (HL) intensity, the fluorescence decay slows down (Fig. 3D–F), similar to fluorescence decay kinetics observed for the solubilised PSII particles (see above) and in vivo (e.g. [6]). This effect is enhanced in the presence of DCMU and reduced in the presence of $K_3Fe(CN)_3$ (see Supplementary Table S1). The fastest lifetime (~0.1 ns) in the global fit originates solely from PSII with open RCs [5,7], so its relative amplitude ($p_{0.1ns}$) is a measure for the fraction of open RCs. Indeed, $p_{0.1ns}$ increases in the presence of $K_3Fe(CN)_3$, and decreases in the presence of DCMU at increased excitation intensity (Table 1). Under all the conditions applied, a significant fraction ($p_{0.1ns} > 0.3$) of RCs remains open. This may be due to the experimental design of FLIM, with a short illumination period (typical pixel dwell time of 50–100 μs), followed by a relatively long dark period (typically ~2 ms). The dark period allows for recovery of RCs to the open state between two consecutive illumination periods. Under all the conditions examined, the fraction of closed RCs in SrPSII is smaller ($p_{0.1ns}$ larger) or equal to that in CaPSII (Table 3), indicating that CaPSII RCs close more readily than SrPSII RCs, analogous to solubilised PSII particles (see above and Fig. 2).

4. Conclusions

4.1. Comparison between CaPSII and SrPSII

Fluorescence decay kinetics of solubilised CaPSII and SrPSII particles with open RCs are very similar (Figs. 1, 4 and Table 1), albeit with a slightly faster decay for CaPSII as compared to SrPSII (4 ps shorter average fluorescence lifetime). At higher excitation intensity and in the presence of the electron transfer inhibitor DCMU (closed RCs) the decay slows down significantly. As full RC closure could not be achieved, a direct comparison of the fluorescence decay kinetics in CaPSII and SrPSII closed states was not possible. Nevertheless, RCs in CaPSII appear more readily closed than those in SrPSII (Fig. 2 and Table 3). This may be related to the apparent differences of the forward and backward electron transfer rates between S_2 and Q_A^- upon substitution of Ca^{2+} with Sr^{2+} in the OEC [40,49], as a result of perturbation of the geometry, as well as the substrate water and carboxylate ligand binding within the catalytic centre of PSII during water splitting cycle [15,26,28,54].

We conclude that substitution of Ca^{2+} by Sr^{2+} in the OEC has only a minor secondary effect on the excited state kinetics of PSII particles, but rather appears to affect electron transfer kinetics (in agreement with [40,49]).

Table 3
Fit results of fluorescence decay curves of CaPSII and SrPSII crystals. Amplitude of the 0.1 ns component ($p_{0.1ns}$) of the fit in Table 2 and Supplementary Table S1, for different experimental conditions.

Buffer additives	CaPSII		SrPSII	
	LL[a]	HL[b]	LL	HL
None	0.73	0.38	0.66	0.36
4 mM $K_3Fe(CN)_3$	0.93	0.48	0.91	0.60
10 μM DCMU	0.55	0.34	0.60	0.37

[a] Lowest excitation intensity.
[b] Highest excitation intensity.

4.2. Comparison between crystallised and solubilised PSII particles

Fluorescence decay curves of crystallised and solubilised PSII particles with open RCs are indistinguishable (Fig. 4), as confirmed by comparing the fitted fluorescence lifetimes and amplitudes (Tables 1 and 2), despite the reduced signal-to-noise ratio in the crystal experiments. Analogous to the solubilised particles, upon RC closure (by increasing excitation intensity and inhibiting the Q_B site with DCMU), the fluorescence decay of the crystallised PSII slows down. Moreover, as for solubilised particles, closing of the RCs seems more efficient in CaPSII than SrPSII, as probed by the amplitude of the shortest lifetime (Table 3), which may be due to the stabilisation of the $S_2Q_A^-$ charge-separated state for SrPSII, leading to an improved recovery of the SrPSII RC to the open state when compared to the native counterpart.

We conclude that crystallisation of the two types of PSII particles does not significantly affect the excited-state kinetics in this photocatalytically active complex. Thus, it is appropriate to use the structure obtained from PSII core particles for theoretical modelling of energy transfer and trapping, in contrast to trimeric LHCII antenna of spinach [37,39] and pea [38], in which the average fluorescence lifetime is approximately five-fold shorter for the crystallised complex as compared to its solubilised counterpart.

Acknowledgements

BvO acknowledges support by the Netherlands Organisation for Scientific Research (NWO) through a Veni grant. JK gratefully acknowledges the support from the Polish Ministry of Science and Higher Education and the European Science Foundation (grant no. 844/N-ESFEuroSolarFuels/10/2011/0). HvA acknowledges support by the Stichting voor Fundamenteel onderzoek der Materie (FOM), which is financially supported by the Netherlands Organisation for Scientific Research (NWO). JB and JK acknowledge financial support for this work from the Biotechnology and Biological Science Research Council (BBSRC).

Appendix A. Supplementary data

Supplementary data to this article can be found online at http://dx.doi.org/10.1016/j.bbabio.2013.11.008.

References

[1] G.H. Schatz, H. Brock, A.R. Holzwarth, Picosecond kinetics of fluorescence and absorbance changes in photosystem II particles excited at low photon density, Proc. Natl. Acad. Sci. 84 (1987) 8414–8418.
[2] G.H. Schatz, H. Brock, A.R. Holzwarth, Kinetic and energetic model for the primary processes in photosystem II, Biophys. J. 54 (1988) 397–405.
[3] G. Renger, H.J. Eckert, A. Bergmann, J. Bernarding, B. Liu, A. Napiwotzki, et al., Fluorescence and spectroscopic studies of exciton trapping and electron transfer in photosystem II of higher plants, Funct. Plant Biol. 22 (1995) 167–181.
[4] N.P. Pawlowicz, M.-L. Groot, I.H.M. van Stokkum, J. Breton, R. van Grondelle, Charge separation and energy transfer in the photosystem II core complex studied by femtosecond midinfrared spectroscopy, Biophys. J. 93 (2007) 2732–2742.
[5] Y. Miloslavina, M. Szczepaniak, M.G. Müller, J. Sander, M. Nowaczyk, M. Rögner, et al., Charge separation kinetics in intact photosystem II core particles is trap-limited. A picosecond fluorescence study, Biochemistry 45 (2006) 2436–2442.
[6] L. Tian, S. Farooq, H. van Amerongen, Probing the picosecond kinetics of the photosystem II core complex in vivo, Phys. Chem. Chem. Phys. 15 (2013) 3146–3154.
[7] C.D. van der Weij-de Wit, J.P. Dekker, R. van Grondelle, I.H.M. van Stokkum, R. Van Grondelle, I.H.M. Van Stokkum, Charge separation is virtually irreversible in photosystem II core complexes with oxidized primary quinone acceptor, J. Phys. Chem. A 115 (2011) 3947–3956.
[8] M. Szczepaniak, J. Sander, M. Nowaczyk, M.G. Müller, M. Rögner, a R. Holzwarth, Charge separation, stabilization, and protein relaxation in photosystem II core particles with closed reaction center, Biophys. J. 96 (2009) 621–631.
[9] Y. Umena, K. Kawakami, J.-R. Shen, N. Kamiya, Crystal structure of oxygen-evolving photosystem II at a resolution of 1.9 Å, Nature 473 (2011) 55–60.
[10] A. Guskov, J. Kern, A. Gabdulkhakov, M. Broser, A. Zouni, W. Saenger, Cyanobacterial photosystem II at 2.9-A resolution and the role of quinones, lipids, channels and chloride, Nat. Struct. Mol. Biol. 16 (2009) 334–342.
[11] B. Loll, J. Kern, W. Saenger, A. Zouni, J. Biesiadka, Towards complete cofactor arrangement in the 3.0 A resolution structure of photosystem II, Nature 438 (2005) 1040–1044.
[12] K.N. Ferreira, T.M. Iverson, K. Maghlaoui, J. Barber, S. Iwata, Architecture of the photosynthetic oxygen-evolving center, Science 303 (2004) 1831–1838.
[13] N. Kamiya, J.-R. Shen, Crystal structure of oxygen-evolving photosystem II from *Thermosynechococcus vulcanus* at 3.7-A resolution, Proc. Natl. Acad. Sci. U. S. A. 100 (2003) 98–103.
[14] A. Zouni, H.T. Witt, J. Kern, P. Fromme, N. Krauss, W. Saenger, et al., Crystal structure of photosystem II from *Synechococcus elongatus* at 3.8 A resolution, Nature 409 (2001) 739–743.
[15] F.H.M. Koua, Y. Umena, K. Kawakami, J.-R. Shen, Structure of Sr-substituted photosystem II at 2.1 A resolution and its implications in the mechanism of water oxidation, Proc. Natl. Acad. Sci. U. S. A. 110 (2013) 3889–3894.
[16] J.W. Murray, K. Maghlaoui, J. Kargul, N. Ishida, T.-L. Lai, A.W. Rutherford, et al., X-ray crystallography identifies two chloride binding sites in the oxygen evolving centre of Photosystem II, Energy Environ. Sci. 1 (2008) 161.
[17] J.W. Murray, K. Maghlaoui, J. Kargul, M. Sugiura, J. Barber, Analysis of xenon binding to photosystem II by X-ray crystallography, Photosynth. Res. 98 (2008) 523–527.
[18] S.I. Allakhverdiev, V.K. Yachandra, J. Yano, Calcium in the oxygen-evolving complex: structural and mechanistic role determined by X-ray spectroscopy, J. Photochem. Photobiol. B Biol. 104 (2011) 51–59.
[19] M. Haumann, C. Müller, P. Liebisch, L. Iuzzolino, J. Dittmer, M. Grabolle, et al., Structural and oxidation state changes of the photosystem II manganese complex in four transitions of the water oxidation cycle ($S_0 \rightarrow S_1$, $S_1 \rightarrow S_2$, $S_2 \rightarrow S_3$, and $S_{3,4} \rightarrow S_0$) characterized by X-ray absorption spectroscopy at 20 K and room temperature, Biochemistry 44 (2005) 1894–1908.
[20] C. Glöckner, J. Kern, M. Broser, A. Zouni, V. Yachandra, J. Yano, Structural changes of the oxygen evolving complex in photosystem II during the catalytic cycle, J. Biol. Chem. (2013), http://dx.doi.org/10.1074/jbcM3.476622 (in press).
[21] J. Yano, J. Kern, K. Sauer, M.J. Latimer, Y. Pushkar, J. Biesiadka, et al., Where water is oxidized to dioxygen: structure of the photosynthetic Mn4Ca cluster, Science 314 (2006) 821–825.
[22] Y. Pushkar, J. Yano, K. Sauer, A. Boussac, V.K. Yachandra, Structural changes in the Mn4Ca cluster and the mechanism of photosynthetic water splitting, Proc. Natl. Acad. Sci. 105 (2008) 1879–1884.
[23] H. Dau, A. Grundmeier, P. Loja, M. Haumann, On the structure of the manganese complex of photosystem II: extended-range EXAFS data and specific atomic-resolution models for four S-states, Philos. Trans. R. Soc. Lond. B Biol. Sci. 363 (2008) 1237–1243(discussion 1243–4).
[24] N. Cox, L. Rapatskiy, J.-H. Su, D.A. Pantazis, M. Sugiura, L. Kulik, et al., Effect of Ca2+/Sr2+ substitution on the electronic structure of the oxygen-evolving complex of photosystem II: a combined multifrequency EPR, 55Mn-ENDOR, and DFT study of the S2 state, J. Am. Chem. Soc. 133 (2011) 3635–3648.
[25] M. Pérez Navarro, W.M. Ames, H. Nilsson, T. Lohmiller, D.A. Pantazis, L. Rapatskiy, et al., Ammonia binding to the oxygen-evolving complex of photosystem II identifies the solvent-exchangeable oxygen bridge (μ-oxo) of the manganese tetramer, Proc. Natl. Acad. Sci. 110 (2013) 15561–15566.
[26] M.A. Strickler, L.M. Walker, W. Hillier, R.J. Debus, Evidence from biosynthetically incorporated strontium and FTIR difference spectroscopy that the C-terminus of the D1 polypeptide of photosystem II does not ligate calcium, Biochemistry 44 (2005) 8571–8577.
[27] B.C. Polander, B.A. Barry, Detection of an intermediary, protonated water cluster in photosynthetic oxygen evolution, Proc. Natl. Acad. Sci. (2013), http://dx.doi.org/10.1073/pnas.1306532110 (in press).
[28] H. Suzuki, Y. Taguchi, M. Sugiura, A. Boussac, T. Noguchi, Structural perturbation of the carboxylate ligands to the manganese cluster upon Ca2+/Sr2+ exchange in the S-state cycle of photosynthetic oxygen evolution as studied by flash-induced FTIR difference spectroscopy, Biochemistry 45 (2006) 13454–13464.
[29] J.R. Lakowicz, Time-resolved protein fluorescence, in: J.R. Lakowicz (Ed.), 3rd ed., Princ. Fluoresc. Spectrosc.Springer, US, 2000, pp. 577–606.
[30] V.I. Novoderezhkin, R. van Grondelle, Physical origins and models of energy transfer in photosynthetic light-harvesting, Phys. Chem. Chem. Phys. 12 (2010) 7352–7365.
[31] R. van Grondelle, V.I. Novoderezhkin, Energy transfer in photosynthesis: experimental insights and quantitative models, Phys. Chem. Chem. Phys. 8 (2006) 793–807.
[32] R. Croce, H. van Amerongen, Light-harvesting and structural organization of Photosystem II: from individual complexes to thylakoid membrane, J. Photochem. Photobiol. B 104 (2011) 142–153.
[33] I.H.M. van Stokkum, D.S. Larsen, R. van Grondelle, Global and target analysis of time-resolved spectra, Biochim. Biophys. Acta 1657 (2004) 82–104.
[34] C. Ruckebusch, M. Sliwa, P. Pernot, a. de Juan, R. Tauler, Comprehensive data analysis of femtosecond transient absorption spectra: a review, J. Photochem. Photobiol. C 13 (2012) 1–27.
[35] I.H.M. van Stokkum, B. van Oort, F. van Mourik, B. Gobets, H. van Amerongen, Govindjee, (Sub)-picosecond spectral evolution of fluorescence studied with a synchroscan streak-camera system and target analysis, in: T.J. Aartsma, J. Matysik (Eds.), Biophys. Tech. Photosynth., vol. II, Springer, Dordrecht, 2008, pp. 223–240.
[36] H. van Amerongen, R. Croce, Light harvesting in photosystem II, Photosynth. Res. 116 (2013) 251–263.
[37] A.A. Pascal, Z.F. Liu, K. Broess, B. van Oort, H. van Amerongen, C. Wang, et al., Molecular basis of photoprotection and control of photosynthetic light-harvesting, Nature 436 (2005) 134–137.
[38] T. Barros, A. Royant, J. Standfuss, A. Dreuw, W. Kuhlbrandt, Crystal structure of plant light-harvesting complex shows the active, energy-transmitting state, EMBO J. 28 (2009) 298–306.
[39] B. van Oort, A. Marechal, A.V. Ruban, B. Robert, A.A. Pascal, N.C.A. de Ruijter, et al., Different crystal morphologies lead to slightly different conformations of light-harvesting complex II as monitored by variations of the intrinsic fluorescence lifetime, Phys. Chem. Chem. Phys. 13 (2011) 12614–12622.
[40] J. Kargul, K. Maghlaoui, J.W. Murray, Z. Deak, A. Boussac, W.A. Rutherford, et al., Purification, crystallization and X-ray diffraction analyses of the *T. elongatus* PSII core dimer with strontium replacing calcium in the oxygen-evolving complex, Biochim. Biophys. Acta Bioenerg. 1767 (2007) 404–413.
[41] R. Krivanek, J. Kern, A. Zouni, H. Dau, M. Haumann, Spare quinones in the QB cavity of crystallized photosystem II from *Thermosynechococcus elongatus*, Biochim. Biophys. Acta Bioenerg. 1767 (2007) 520–527.
[42] A. Royant, P. Carpentier, J. Ohana, J. McGeehan, B. Paetzold, M. Noirclerc-Savoye, et al., Advances in spectroscopic methods for biological crystals. 1. Fluorescence lifetime measurements, J. Appl. Crystallogr. 40 (2007) 1105–1112.
[43] B. van Oort, A. Amunts, J.W. Borst, A. van Hoek, N. Nelson, H. van Amerongen, et al., Picosecond fluorescence of intact and dissolved PSI-LHCI crystals, Biophys. J. 95 (2008) 5851–5861.
[44] J.W. Borst, M.A. Hink, A. van Hoek, A.J.W.G. Visser, Effects of refractive index and viscosity on fluorescence and anisotropy decays of enhanced cyan and yellow fluorescent proteins, J. Fluoresc. 15 (2005) 153–160.
[45] A. van Hoek, A.J.W.G. Visser, Artefact and distortion sources in time correlated single photon counting, Anal. Instrum. 14 (1985) 359–378.
[46] A.V. Digris, V.V. Skakoun, E.G. Novikov, A. van Hoek, A. Claiborne, A.J.W.G. Visser, Thermal stability of a flavoprotein assessed from associative analysis of polarized time-resolved fluorescence spectroscopy, Eur. Biophys. J. 28 (1999) 526–531.
[47] N. Boens, M. Ameloot, I. Yamazaki, F.C. De Schryver, On the use and the performance of the delta function convolution method for the estimation of fluorescence decay parameters, Chem. Phys. 121 (1988) 73–86.
[48] E. Russinova, J.-W. Borst, M. Kwaaitaal, A. Caño-Delgado, Y. Yin, J. Chory, et al., Heterodimerization and endocytosis of *Arabidopsis brassinosteroid* receptors BRI1 and AtSERK3 (BAK1), Plant Cell 16 (2004) 3216–3229.
[49] A. Boussac, F. Rappaport, P. Carrier, J.M. Verbavatz, R. Gobin, D. Kirilovsky, et al., Biosynthetic Ca2+/Sr2+ exchange in the photosystem II oxygen-evolving enzyme of *Thermosynechococcus elongatus*, J. Biol. Chem. 279 (2004) 22809–22819.
[50] G. Brudvig, C.F. Yocum, The calcium and chloride requirements of the O2 evolving complex, Coord. Chem. Rev. 252 (2008) 296–305.
[51] T. Ono, A. Rompel, H. Mino, N. Chiba, Ca2+ function in photosynthetic oxygen evolution studied by alkali metal cations substitution, Biophys. J. 81 (2001) 1831–1840.
[52] J.S. Vrettos, D.A. Stone, G.W. Brudvig, Quantifying the ion selectivity of the Ca 2+ site in photosystem II: evidence for direct involvement of Ca^{2+} in O_2 formation, Biochemistry 40 (2001) 7937–7945.
[53] A. Boussac, A.W. Rutherford, Nature of the inhibition of the oxygen-evolving enzyme of photosystem II induced by sodium chloride washing and reversed by the addition of calcium(2+) or strontium(2+), Biochemistry 27 (1988) 3476–3483.
[54] B.C. Polander, B.A. Barry, Calcium, strontium, and protein dynamics during the S2 to S3 transition in the photosynthetic oxygen-evolving cycle, J. Phys. Chem. Lett. 4 (2013) 3356–3362.
[55] J.M. Beechem, E. Gratton, M. Ameloot, J.R. Knutson, L. Brand, J.R. Lakowicz, The global analysis of fluorescence intensity and anisotropy decay data: second-generation theory and programs, in: J.R. Lakowicz (Ed.), Top. Fluoresc. Spectrosc, 2nd ed., Princ., vol. 2, Springer, US, New York, Boston, Dordrecht, London, Moscow, 2002, pp. 241–305.